

# Enhanced performance in the direct electrocatalytic synthesis of ammonia from N<sub>2</sub> and H<sub>2</sub>O by an in-situ electrochemical activation of CNT-supported iron oxide nanoparticles<sup>†</sup>

Shiming Chen<sup>a,b,\*</sup>, Siglinda Perathoner<sup>a</sup>, Claudio Ampelli<sup>a</sup>, Hua Wei<sup>a</sup>,  
Salvatore Abate<sup>a</sup>, Bingsen Zhang<sup>c</sup>, Gabriele Centi<sup>d,\*</sup>

<sup>a</sup>Dept. ChimBioFarAM, V.le F. Stagno D'Alcontres 31, 98166 Messina, Italy

<sup>b</sup>Dalian Institute of Chemical Physics, Chinese Academy of Sciences, Dalian 116023, Liaoning, China

<sup>c</sup>Catalysis and Materials Division, Institute of Metal Research, Chinese Academy of Sciences (IMR CAS),  
Shenyang 110016, Liaoning, China

<sup>d</sup>Dept. MIFT (Industrial University of Messina, ERIC aisbl and INSTM/CASPE V.le F. Stagno D'Alcontres  
31, 98166 Messina, Italy

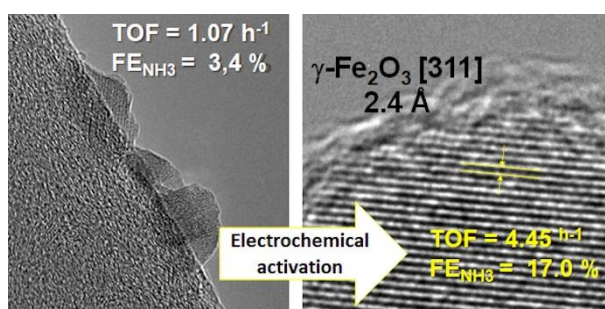
<sup>†</sup> In memory of Dangsheng Su (DICP, Dalian - China) who contributed to starting this study and which legacy is still a great source of inspiration for all of us.

\*Corresponding authors.

E-mail addresses: [centi@unime.it](mailto:centi@unime.it) (G. Centi), [chenshiming@dicp.ac.cn](mailto:chenshiming@dicp.ac.cn) (S. Chen).

**Keyword:** Ammonia direct synthesis; Electrochemical activation; Heterogeneous catalysis; Active sites; N<sub>2</sub> electrocatalytic conversion

## Graphical Abstract:



Electrochemical method to prepare high performance catalysts for direct synthesis of ammonia from N<sub>2</sub> and H<sub>2</sub>O at ambient temperature/pressure.

<sup>†</sup>

## ABSTRACT

The direct electrocatalytic synthesis of ammonia from  $N_2$  and  $H_2O$  by using renewable energy sources and ambient pressure/temperature operations is a breakthrough technology, which can reduce by over 90% the greenhouse gas emissions of this chemical and energy storage process. We report here an in-situ electrochemical activation method to prepare  $Fe_2O_3$ -CNT (iron oxide on carbon nanotubes) electrocatalysts for the direct ammonia synthesis from  $N_2$  and  $H_2O$ . The in-situ electrochemical activation leads to a large increase of the ammonia formation rate and Faradaic efficiency which reach the surprising high values of  $41.6 \mu g \text{ mg}_{\text{cat}}^{-1} \text{ h}^{-1}$  and 17%, respectively, for an in-situ activation of 3 h, among the highest values reported so far for non-precious metal catalysts that use a continuous-flow polymer-electrolyte-membrane cell and gas-phase operations for the ammonia synthesis hemicell. The electrocatalyst was stable at least 12 h at the working conditions. Tests by switching  $N_2$  to Ar evidence that ammonia was formed from the gas-phase nitrogen. The analysis of the changes of reactivity and of the electrocatalyst characteristics as a function of the time of activation indicates a linear relationship between the ammonia formation rate and a specific XPS (X-ray-photoelectron spectroscopy) oxygen signal related to  $O^{2-}$  in iron-oxide species. This results together with characterization data by TEM and XRD suggest that the iron species active in the direct and selective synthesis of ammonia is a maghemite-type iron oxide, and this transformation from the initial hematite is responsible for the in-situ enhancement of 3-4 times of the TOF (turnover frequency) and  $NH_3$  Faradaic efficiency. This transformation is likely related to the stabilization of the maghemite species at CNT defect sites, although for longer times of preactivation a sintering occurs with a loss of performances.

## 1. Introduction

Ammonia synthesis is the largest-scale chemical process with the highest impact on greenhouse gas emissions, about 350 Mt CO<sub>2</sub> emissions worldwide. This value could be decreased by over 90% in a direct electrocatalytic process using N<sub>2</sub>, H<sub>2</sub>O and renewable energy as input sources. In fact, CO<sub>2</sub> emissions are 1.83 t<sub>CO2</sub>/t<sub>NH3</sub> in the actual ammonia production scheme (via natural gas steam reforming followed by NH<sub>3</sub> synthesis), while the total footprint of the direct electrocatalytic route could be estimated in 0.12 t<sub>CO2eq</sub>/t<sub>NH3</sub> [1]. Implementing this technology will thus result in a breakthrough change towards a sustainable, low-carbon chemical production based on the use of renewable energy sources [2–6]. There is thus a rising interest in fossil-fuel-free direct ammonia synthesis [7–33], both as alternative way to commercial high temperature/pressure catalytic synthesis from CH<sub>4</sub> and air (Haber-Bosch process), and as process for using ammonia as a chemical energy vector.

We reported recently that electrocatalysts based on iron nanoparticles supported on carbon nanotubes (Fe<sub>2</sub>O<sub>3</sub>-CNT) are effective and stable electrocatalysts in this process [34]. While other types of electrocatalysts have been also reported [7–33], the interest on these electrocatalysts is that iron is also the active element in thermal industrial ammonia catalysts working at high temperature and pressure (about 400–450 °C and 10–30 MPa) [35]. In these catalysts, the starting phase is iron-oxide, which is then reduced to the metallic form (fused iron) during the initial pre-reduction step. There is a good agreement that in these catalysts the mechanism proceeds via first the N<sub>2</sub> dissociative chemisorption [36,37]. An analogy in the reaction mechanisms between thermal catalysis and electrocatalysis was postulated [38], but other authors indicate the presence of a different reaction mechanism. For example, Bao et al. [19] proposed by theoretical studies a reductive adsorption of N<sub>2</sub> to form N<sub>2</sub>H• species as rate determining step in the electrocatalytic reduction of N<sub>2</sub> to NH<sub>3</sub> on gold nanorods. Nørskov et al. [20,39] pointed out that the stability of N<sub>2</sub>H• adsorbate is a key for the low-temperature electrocatalytic production of NH<sub>3</sub> from N<sub>2</sub>. Both these theoretical studies proposed that the rate determining step is the hydrogen addition to an undissociated chemisorbed N<sub>2</sub> molecule (similar to what present in the *Nitrogenase* enzyme [40]), but there are no experimental results which proof the proposed reaction mechanism. Based on operando EXAFS evidences that similar electrocatalysts transform in situ (during CO<sub>2</sub> electrocatalytic reduction) to a FeOOH type of species stabilized at carbon defect sites [41], we proposed that a similar species is also active in direct N<sub>2</sub> conversion to NH<sub>3</sub> through a multi-electron/proton transfer [42]. Cui et al. [9] reported for unsupported iron-oxide (α-Fe<sub>2</sub>O<sub>3</sub>) electrocatalysts that both the NH<sub>3</sub> yield and faradaic efficiency can be largely improved by creation of surface oxygen vacancies in the hematite nanoparticles, although

a fast deactivation is present. Jin et al. [8] also proposed that vacancies in 2D layered  $W_2N_3$  nanosheet are the active sites for nitrogen reduction reaction (NRR). They suggest that these vacancies are stable by virtue of the high valence state of tungsten atoms and 2D confinement effect. These vacancies provide an electron-deficient environment which not only facilitates nitrogen adsorption, but also lowers the thermodynamic limiting potential of NRR. However, the presence of already N in the electrocatalyst may make difficult to discriminate whether nitrogen in the formed  $NH_3$  derives only from gaseous  $N_2$ , a crucial aspect to demonstrate as remarked in the tutorial review by Tang and Qiao [7].

We noted that iron-oxide ( $Fe_2O_3$ ) nanoparticles (supported over carbon nanotubes - CNTs) may transform during the electrocatalytic reaction under some conditions. This offers both the possibility to use this in-situ transformation to prepare improved electrocatalysts and to determine more precisely the nature of the active species in  $NH_3$  direct synthesis through the determination of relationships between rate of ammonia formation and specific electrocatalyst active species. This allows to find correlations on the same catalyst, rather than through the comparison of different catalysts. It will also allow to understand whether the activation of iron-oxide observed in the unsupported hematite [8] is related to the generation of surface vacancies or to a surface phase transformation, because the use of CNT as support will allow to stabilize smaller iron nanoparticles with respect to unsupported iron-oxide case and thus to not limit to surface the structural reorganization.

This work thus aims from one side to evidence that an in-situ electrochemical activation is a good method to enhance significantly the performances of  $Fe_2O_3$ -CNT electrocatalysts active in the direct ammonia synthesis and that the characterization of the electrocatalysts during this activation procedure provides relevant indications about the nature of the active sites in ammonia direct synthesis and in turn on the reaction mechanism, including indications about the differences between electrocatalysis and thermal catalysis of iron catalysts for ammonia synthesis.

## 2. Experimental

### 2.1 Materials and chemicals

Pyrograph®-III, CNT PR-24XT were used as carbon nanotubes (CNTs). A commercial gas diffusion layer (SIGRACET GDL 29BC) supplied by SGL Group and Nafion®115 membrane (Sigma Aldrich) were used to prepare the electrode. Nafion solution (10 wt%) was used to prepare the catalyst ink. Iron (III) nitrate nonahydrate (Sigma Aldrich, 99.9% purity) was used as precursor during the  $Fe_2O_3$ -CNT synthesis.

## 2.2 Preparation of the electrodes

The preparation of electrodes can be summarized in the following steps.

### 2.2.1 Synthesis of the initial electrocatalyst (*Fresh-Fe<sub>2</sub>O<sub>3</sub>-CNT*)

Synthesis of the initial electrocatalyst starts with the pretreatment of commercial CNTs in order to purify and create surface oxygen functionalities (o-CNT). Briefly, 1 g of CNTs was suspended in 100 mL concentrated HNO<sub>3</sub> (Sigma Aldrich, 65%) and treated at 120 °C for 2 h in a reflux setup. The suspension was filtered and washed with deionized (DI) water until neutral pH. The sample was then dried at 80 °C overnight and grounded to obtain homogeneous o-CNT.

o-CNT and Fe(NO<sub>3</sub>)<sub>3</sub> were dissolved in 25 mL of deionized water with 1 mL ethanol glycol. The mixture was then sonicated for 30 min and pH was adjusted to 8 with a 5% ammonia solution. After adjusting the pH, the solvent is eliminated and the sample then dried at 120 °C. The dried sample was then calcined for 2 h at 400 °C in a tubular furnace under He flow. Finally, the obtained sample was grounded to get a homogeneous catalyst. A loading of 30 wt% of iron was utilized in the tests reported here, being this amount optimized to give the higher rate in ammonia direct synthesis from N<sub>2</sub>. This sample is indicated hereinafter as *Fresh-Fe<sub>2</sub>O<sub>3</sub>-CNT*.

### 2.2.2 *In-situ* activation of the initial electrocatalyst

5 mg of the *Fresh-Fe<sub>2</sub>O<sub>3</sub>-CNT* was suspended in a 5 mL ethanol. The solution was sonicated for 90 min to get a homogeneous mixture. Finally, the ink solution was uniformly loaded by spray drying on a carbon paper (Sigracet 29BC) with a loading 0.05 mg·cm<sup>-2</sup>, i.e. about 0.01 mg<sub>Fe<sub>2</sub>O<sub>3</sub></sub>·cm<sup>-2</sup>. It was then introduced in the reactor to activate the electrocatalyst at the potential of -1.0 V vs. RHE for a given time. Finally, the activated Fe<sub>2</sub>O<sub>3</sub>-CNT was removed from the carbon paper, filtered and washed with deionized water to remove the amorphous carbon (from Carbon paper) and the iron that was not strongly interacting with CNTs. These samples were dried at 80 °C for 12 h.

### 2.2.3 Preparation of the electrodes with the *in-situ* activated electrocatalysts

0.1 mg of the as activated electrocatalysts are suspended in a 1 mL ethanol and 10 μL Nafion solution. This ink is sonicated for 90 min to obtain a homogeneous mixture. Finally, the ink is deposited uniformly by spray drying on the gas diffusion layer (GDL 2 cm<sup>2</sup>) heated on a hot plate at 100 °C. The GDL with the activated electrocatalyst is then stored in an oven at 80 °C overnights. The GDL (on which the electrocatalyst was deposited on the side that will be joined with Nafion) and a purified Nafion membrane is then hot pressed together at 80 atm and 130 °C for 30 s. This assembled composite electrode is then mounted in the electrocatalytic flow reactor which operates in the absence of a liquid electrolyte in the chamber where ammonia synthesis is realized (see later and Supplementary

Information). These samples are indicated as activated 1 h, activated 3 h, activated 6 h and activated 24 h respectively.

### 2.3 Characterization of catalysts

XRD (X-ray diffraction) measurements were carried out using a Bruker D2-Phaser diffractometer operating with Cu  $K_{\alpha}$  radiation at 30 kV and 10 mA with 3 mm scattering scale. The  $2\theta$  range explored was  $10^{\circ}$ – $90^{\circ}$ .

The Fe<sub>2</sub>O<sub>3</sub>-CNT electrocatalyst, fresh and after 1 h, 3 h, 6 h and 24 h of tests in the described conditions, were characterized by transmission electron microscopy (TEM), after be ultrasonical dispersed in ethanol, and placed then as a drop of solution on a holey C/Cu TEM grid. FEI Tecnai G2 F20 and Philips CM 200 FEG microscopes operating at 200 kV were used.

The XPS spectra were recorded using a PHI VersaProbe II analyser (Physical Electronics). The results were analysed by using Multipak (Matlab) software. Position of XPS peaks was referred to graphite carbon C 1s, whose energy was taken equal to 284.8 eV.

### 2.4 Electrocatalytic apparatus and testing conditions

All the electrochemical measurements were carried out at 20 °C using a potentiostat/galvanostat AMEL 2551. A Pt wire was used as the counter electrode. All the potentials were measured against Ag/AgCl reference electrode (3 M). A non-conventional type of electrocatalytic cell (operating at atmospheric pressure and room temperature) was developed for these tests, where the solid membrane-electrode assembly separates gas and liquid zones. The gas zone is where the ammonia synthesis occurs, while the liquid zone (the liquid term refers to the presence of a liquid electrolyte) is where the water electrolysis occurs to generate the protons/electrons used in the cathodic (gas) zone to reduce N<sub>2</sub> to NH<sub>3</sub>. Further details and a scheme of the electrocatalytic reactor are reported in the Supplementary Information. 0.5 M KOH was used as electrolyte. Supplementary Information reports the method to calculate the rate of ammonia formation and Faradaic selectivity.

The solid zone consists of a Nafion membrane, a catalyst layer and a gas diffusion layer (GDL). The size of the electrode was 2 cm<sup>2</sup> containing 0.1 mg of the electrocatalysts. The reactant N<sub>2</sub> (acting both as reactant and transport gas for the generated ammonia) was continuously fed (20 mL/min of N<sub>2</sub> with purity, 99.9999%), and the flow coming out from the electrocatalytic reactor outlet (containing a mixture of N<sub>2</sub> and ammonia) is sent to a liquid absorber containing a 0.001 M H<sub>2</sub>SO<sub>4</sub> solution. The amount of ammonia formed is monitored by a spectrophotometric method with a highly sensitive and very specific procedure (see Supplementary part). Average experimental error is  $\pm 5\%$ .

The N<sub>2</sub> flow is introduced to the cathode part of the cell 30 min before starting the application of

the potential and then continuously fed till the end of the electrocatalytic test (from 2 to 24 h). To check stability of operations to on/off applications of the potential, an important aspect of stability for using this technology to produce ammonia as an energy vector to transport renewable energy from remote areas, the behaviour during a series of consecutive cycles was also tested (see later). Each cycle consists in flushing the electrocatalytic ammonia synthesis hemicell with N<sub>2</sub> for 30 min, and then application of the constant potential for 2 h.

A series of tests were made to confirm that NH<sub>3</sub> is formed from the gas phase N<sub>2</sub> and not from other N-species present in the electrode or electrolyte. In these tests, N<sub>2</sub> feed was switched to an Ar flow in order to confirm that ammonia derives from N<sub>2</sub>. Additional blank tests regard checking whether the ammonia detected forms by the electrocatalytic reduction of N<sub>2</sub>, rather than from a catalytic reaction. In these tests, no potential is applied, but the N<sub>2</sub> flow in the ammonia synthesis hemicell is substituted with a N<sub>2</sub> + H<sub>2</sub> (1:3) ratio, to compensate that without application of the potential, water electrolysis does not occur in the liquid hemicell and thus H<sup>+</sup>/e<sup>-</sup> are not available for the electrocatalytic conversion of N<sub>2</sub> to NH<sub>3</sub>.

### 3. Results

#### 3.1 *In-situ activation procedure and effect on iron species*

The starting carbon nanotubes (CNTs) were first functionalized by oxidative treatment (o-CNT). This pretreatment is necessary to obtain a good and stable dispersion of the iron oxide nanoparticles which result located mainly on the external surface of the CNTs, as evidenced by TEM images reported in the Supplementary Part (Fig. S6). The presence of α-Fe<sub>2</sub>O<sub>3</sub> (hematite) is confirmed by interplanar crystal spacing measured by TEM (0.25 nm) which match with the crystal face [311] of iron(III) oxide (Fig. S5 in the supplementary part). Numerous particles with the diameter of about 1 nm were observed by TEM and STEM, and even a larger number of nano-sized particles were observed by Energy dispersive X-ray spectroscopy (EDX) elemental map. Fe and O well distributed all over the carbon nanotubes.

To note that we have avoided to dope the CNT with N, e.g. to use N-CNT, even if better ammonia synthesis rates were obtained by using CNT functionalized with nitrogen, to avoid the possible question whether the source of N for the synthesized ammonia is N<sub>2</sub> or N already present in the electrocatalyst, as remarked by Tang and Qiao [7]. In addition, specific tests were made, as reported later, to demonstrate that NH<sub>3</sub> derives from the reduction of gaseous N<sub>2</sub>. It should be noted, however, that traces of N are present in the activated CNT (o-CNT) (see N1S XPS spectra in Figure S9a of the supplementary part) due to traces of nitric acid (used for the oxidative treatment of pristine CNT).

These traces of nitrogen react with iron to form a Fe-N type species, or possibly this species derives from the use of Fe-nitrate as precursor. This species is present in very small amounts, but it does not change in intensity during the electrocatalytic tests (Figure S9b - supplementary part), thus indicating that do not react in the used reaction conditions.

The *Fresh Fe<sub>2</sub>O<sub>3</sub>-CNT* sample was then activated for 1 h, 3 h, 6 h and 24 h by the in-situ electrochemical procedure detailed in the experimental part. The electrochemical activation was made by applying a potential of -1.0 V. As shown from liner sweep voltammetry (LSV) tests (Fig. S10 - supplementary part), the onset potential for NRR reaction is about -0.25 V, but above potentials more negative of about - 1.2–1.5 V, the side reaction of H<sub>2</sub> formation start to be very large, thus inhibiting the reaction of NH<sub>3</sub> formation. For this reason, the electrocatalytic tests were made at -0.5 V, in order to have a good compromise between rate of reaction (which increases at more negative potential applied) and selectivity to ammonia. However, to accelerate slightly the process, the electrochemical activation procedure was made at -1.0 V, which is nevertheless a voltage at which the side reaction of H<sub>2</sub> formation is still low, as shown by LSV tests.

The process of electrochemical activation is similar to that occurring during the initial hours of the electrocatalytic reaction. However, during the in-situ activation, particularly during the initial hour, part of the iron migrates from CNT to the carbon substrate support. This part of iron, which corresponds to that only weakly interacting with CNT (see later), is removed when the activated Fe<sub>2</sub>O<sub>3</sub>-CNT was separated from the carbon paper as a part of the procedure of activation of the initial electrocatalyst (see the experimental part). This is a main difference of the pre-activation strategy reported here with respect to the NRR tests, besides to the possibility to characterize the electrocatalyst.

These electrocatalysts were characterized by high-resolution transmission electron microscopy (HRTEM) and scanning transmission electron microscopy (STEM). STEM mode provides more accurate information to calculate the particle size distribution (PSD) with respect to HRTEM mode [43]. The PSD statistics was made according to the STEM image and is shown in Figure 1 (right side).

#### FIGURE 1 HERE

The average particle size of *Fresh Fe<sub>2</sub>O<sub>3</sub>-CNT* was 8.97 nm, with a broad distribution ranging from 1 to 30 nm. The iron oxide nanoparticles are located mainly on the external surface of the CNTs, as shown in the STEM images (see Supplementary Information, Fig. S5). The regular fringes observed in the nanoparticle have a spacing of 0.25 nm consistent with the [311] interplanar distance of the hematite ( $\alpha$ -Fe<sub>2</sub>O<sub>3</sub>, see Supplementary Information, Fig. S5a). There are two types of iron-oxide nanoparticles, with the smaller particles interacting at defect sites of the CNT (see Fig. S6 - Supplementary Information).

For the *activated 1h* sample, the larger iron-oxide particles reconstruct in-situ forming smaller particles, homogeneously distributed along the CNTs. The average particle size of the *Activated 1h* sample was 5.22 nm and still a broad particle size distribution is present. However, in *Activated 1h* sample  $\geq 50\%$  of the nanoparticles have size lower than 2–3 nm. The washing procedure after the in-situ activation step largely removes iron species, which amount by weight decreases by over twice with respect to the fresh sample (Fig. 1). The HRTEM images of the *activated 1h* sample (see Fig. S7) evidence a clear change of shape and the analysis of the fringes is indicative of the in-situ transformation, likely to  $\gamma\text{-Fe}_2\text{O}_3$  (maghemite).

The samples *activated 3h* and *activated 24h* have an average particle size of 4.51 nm and 5.49 nm, respectively, but a much smaller narrow particle size distribution. The particles below about 3 nm present in the *activated 1h* sample disappear forming slightly larger particles in the 4–6 nm range. However, minor changes in the distribution are observed in going from *activated 3h* to *activated 24h* samples, indicating that the major changes occur during the first 3 h of activation procedure. The particles were uniformly dispersed on the outer surface of the carbon nanotubes, as shown by STEM images (see Supplementary Information, Fig. S7d).

The iron species of *Fresh Fe<sub>2</sub>O<sub>3</sub>-CNT* is  $\alpha\text{-Fe}_2\text{O}_3$  (hematite) according to X-ray powder diffraction (XRD) and HREM (see Supplementary Information, Fig. S5a). On the contrary, iron-oxide or other iron species were not detected by XRD (Supporting Information, Fig. S4a) in the activated samples, being iron-oxide nanoparticles too small or non-crystalline. The presence, however, is indicated by X-ray photoelectron spectroscopy (XPS - see later) and HREM images (Fig. 1). The iron loading indicated by XPS significantly decreases in passing from the *Fresh Fe<sub>2</sub>O<sub>3</sub>-CNT* to the *Activated 1h* sample (see Table S1 - Supporting Information), in agreement with TEM data (Fig. 1). Part of iron during the first hour of activation moves to amorphous carbon (present in carbon paper) and is then removed during the subsequent procedure of separation of iron-loaded CNTs from the carbon paper support. This is clearly evidenced by the STEM images shown in the Supporting Information (Fig. S7(a) - Supplementary Information). The amount of iron after the first hour of in-situ activation only slightly further decreases for longer activation times, indicating that thus this migration of iron occurs mainly during the first hour of activation.

### 3.2 Change of the electrocatalytic behaviour as a function of the in-situ activation procedure

For the nitrogen reduction reaction (NRR) experiments, electrocatalysts were sprayed on carbon paper (0.1 mg, e.g. 0.03 mg as  $\text{Fe}_2\text{O}_3$ ,  $2\text{ cm}^2$ ) utilized as the working electrode. 0.5 M KOH was used as electrolyte in order to limit the hydrogen evolution reaction which was the side reaction during

NRR. The electrocatalysts with different activation times (*Fresh. Fe<sub>2</sub>O<sub>3</sub>-CNT, activated 1h, 3h, 6h and 24h*) were tested at -0.5 V vs. RHE, 0.5 M KOH. As commented before, this applied potential is above the onset potential (see Fig. S10 - Supplementary Information), but still below when the side reaction of H<sub>2</sub> formation start to be too large. Thus, this potential represents a compromise between rate of formation and Faradaic selectivity to ammonia. The results are shown in Fig. 2.

FIGURE 2 HERE

The highest current density is shown by *Fresh Fe<sub>2</sub>O<sub>3</sub>-CNT*, while the lowest current density by the *activated 24h* sample. The current density in activated samples was about one third of the fresh, while the ammonia formation rate was higher than that of the fresh sample, indicating that the activation procedure induces a significant change in the performances, and specifically largely depresses the side reaction of H<sub>2</sub> formation (HER). However, further transformations occur during the subsequent activation, with the rate of ammonia formation passing from 24.1  $\mu\text{g} \cdot \text{mg}_{\text{cat}}^{-1} \cdot \text{h}^{-1}$  (*Fe<sub>2</sub>O<sub>3</sub>-CNT sample*), to 31.6, 41.4, 17.1 and 7.9  $\mu\text{g} \cdot \text{mg}_{\text{cat}}^{-1} \cdot \text{h}^{-1}$  for the samples activated for 1 h, 3 h, 6 h and 24 h, respectively. The highest ammonia formation rate was observed by the *activated 3h* sample, showing also the highest Faradaic selectivity to ammonia which increases about 5 times with respect to the fresh sample.

As a comparison, Cui et al. [9] reported for unsupported  $\alpha$ -Fe<sub>2</sub>O<sub>3</sub> nanoparticles (hematite), but a potential applied of -0.9 V, an average NH<sub>3</sub> production rate of 0.46  $\mu\text{g} \cdot \text{h}^{-1} \cdot \text{cm}^{-2}$  and an NH<sub>3</sub> Faradaic efficiency (FE) of 6.04%. After 1h of chronoamperometry test, they observed an increased NH<sub>3</sub> production rate of 1.45  $\mu\text{g} \cdot \text{h}^{-1} \cdot \text{cm}^{-2}$  with a NH<sub>3</sub> FE of 8.28%, values dropping to 0.29  $\mu\text{g} \cdot \text{h}^{-1} \cdot \text{cm}^{-2}$  and 2.74 %, respectively, after 16 h of chronoamperometry tests. They indicated that these values were the highest reported so far for non-precious metal catalysts [9]. By using the same units for ammonia production rate, the results shown in Figure 2 indicate an ammonia formation rate of 0.45  $\mu\text{g} \cdot \text{h}^{-1} \cdot \text{cm}^{-2}$  with a NH<sub>3</sub> FE of 3.4% for *Fresh Fe<sub>2</sub>O<sub>3</sub>-CNT* and of 0.78  $\mu\text{g} \cdot \text{h}^{-1} \cdot \text{cm}^{-2}$  with a NH<sub>3</sub> FE of 17.0% for the *activated 3h* sample. Taking into account the higher applied negative potential and especially that Cui et al. [9] used an amount of iron-oxide of 3.4  $\text{mg} \cdot \text{cm}^{-2}$  with respect to about 0.01-0.02  $\text{mg} \cdot \text{cm}^{-2}$  used in our case and furthermore that part of the iron-oxide is removed during the pre-activation procedure, it may be concluded that the reaction rate per amount of iron-oxide is significantly higher in our case, in addition to the about twice higher NH<sub>3</sub> FE for the *activated 3h* sample.

With the assumption that all the iron atoms are active in N<sub>2</sub> reduction to NH<sub>3</sub>, the apparent Turnover Frequency (TOF) may be estimated as a function of time of in-situ activation of the samples (Fig. 3). This represents the minimum TOF value possible, because only a fraction of the iron atoms is present on the surface (on the average between 10 and 30 percentage for the particle distributions

shown in Fig. 1) and only a fraction of these atoms would be likely electrocatalytic active. Thus, the effective TOF is larger, at least one order of magnitude higher. The apparent TOF values estimated, although low, are reasonable by considering ambient temperature and pressure operations.

FIGURE 3 HERE

The plot of TOF versus time of in-situ activation of the electrocatalyst clearly evidences the presence of two type of in-situ transformations of iron-oxide species, the first occurring during the first 3 h, where a clear increase of the activity is evident with the TOF increasing more than 4 times, and a second transformation, for longer times of activation, leading instead to a decrease of TOF. The parallel trend of Faradaic selectivity (Fig. 2), indicates that this is not only an effect of dispersion of iron species, but a change of the type of iron-species, although not evidenced from XRD.

The iron oxide in-situ modification was observed, however, by HRTEM (Fig. 4 and Supplementary Information). The crystalline iron oxide larger particles changes to smaller, non-crystalline particles. These smaller nanoparticles are located at the edge or defect sites of CNT. Due to the stronger interaction between non-crystallized iron oxide and CNT, the electrocatalysts show good stability during the performance tests. Although more results would be necessary to confirm this indication, the HRTEM data are consistent with the in-situ transformation from hematite ( $\alpha$ - $\text{Fe}_2\text{O}_3$ ) to maghemite ( $\gamma$ - $\text{Fe}_2\text{O}_3$ ), likely due to the stabilization effect of interaction with CNT (see Supplementary Information), which could explain the higher specific (per amount of iron-oxide) rate of formation of ammonia in our case with respect to unsupported iron-oxide nanoparticles [9]. Note also that XPS data (Fig. S8 in Supplementary Information) indicates that at the applied potential, metallic Fe is not present for all the pre-activation times. In addition, as commented later, XPS data do not evidence the presence of oxygen vacancies as reported by Cui et al. [9] (a shoulder at 531.3 eV on the main peak at 530.0 eV related to lattice oxygen in hematite), even if unambiguous interpretation is difficult due to the presence of various partially overlapping of O1s signals. HRTEM images also do not provide evidences for the formation of significant amounts of surface lattice defects.

FIGURE 4 HERE

### 3.3 Effect of the potential applied

The effect of the applied potential on the most performing electrocatalyst (*activated 3h* sample) was investigated in the range of -0.8 V–-0.3 V of the applied voltages with respect to reversible hydrogen electrode (RHE). As shown in Fig. 5(a), the current densities are stable for at least 4 h of electrocatalytic tests at all the applied voltages. The current density increases nearly linearly when a

more negative voltage is applied. In contrast, the ammonia formation rate increases initially up to a maximum, decreasing then when the more negative voltages are applied. This is due to the increase of the side reaction of proton/electron recombination to form gaseous H<sub>2</sub>. The highest ammonia formation rate (41.4 μg · mg<sub>cat</sub><sup>-1</sup> · h<sup>-1</sup>) with a Faraday efficiency of 17% was observed at the applied voltage of -0.5 V vs. RHE (Fig. 4b).

FIGURE 5 HERE

### 3.4 Evaluation of the stability

To evaluate stability of the electrocatalytic performances, a series of consecutive cyclic tests were made at the applied voltage of -0.5 V vs. RHE using as electrocatalyst the *activated 3h* sample. This sample was tested in a series of consecutive cycles feeding N<sub>2</sub> (Fig. 6a). Each cycle was of 120 min, then the potential was stopped and a new testing cycle was repeated, in order to check the effect also of on/off procedures. Total test time is 12 h. The average ammonia formation rate and Faradaic selectivity were 40.5 μg · mg<sub>cat</sub><sup>-1</sup> · h<sup>-1</sup> and 16.7%, with an error of about 5%, which indicates a good and stable electrocatalytic behaviour at the applied voltage of -0.5 V vs. RHE for at least 12 h of tests.

FIGURE 6 HERE

### 3.5 Verification that ammonia derives from N<sub>2</sub> reduction

There is often a debate whether the detected ammonia derives from N<sub>2</sub> or possible contaminants present in the electrolyte or electrodes [7]. In order to check this relevant aspect, switch tests from feeding Argon rather than N<sub>2</sub> were made (Fig. 6b). Each cycle, as described in the experimental parts, consists of an initial flushing period of 30 min without application of the potential in order to clean the electrocatalytic flow cell, and then application of the potential for 2 h. This type of test is preferable with respect to those when labelled <sup>15</sup>N<sub>2</sub> is fed, because this type of tests will require to perform tests in a batch or recirculation apparatus, rather than in a continuous electrocatalytic reactor as in tests made in Fig. 6(b). In these tests, 2 testing cycles of 2 h each were initially made feeding N<sub>2</sub>, then the feed was switched to Ar for two additional cycles, and finally the feed was switched again to N<sub>2</sub> and two more cycles were made. Initially, after switching to Ar, some minor amounts of ammonia were still detected (Fig. 6b), but which disappear in the further cycle, indicating that these are due to some ammonia still remaining adsorbed on the electrocatalytic reactor. However, the strong decrease with respect to when N<sub>2</sub> is fed, and the further decrease, in the second testing cycle with the Ar feed, clearly points out that ammonia forms from gaseous N<sub>2</sub> reduction on the electrode. In order to further verify this point, and check whether the NH<sub>3</sub> could derive from the small traces of N present

in the electrocatalysts (see XPS data in Fig. S9 - Supplementary Information) due to the oxidative treatment of CNT with nitric acid and the use of iron-nitrate as precursor to load iron on CNTs, a further test was made (not reported for conciseness), in which the two cycles with Ar were made initially (1<sup>st</sup> and 2<sup>nd</sup> cycles) followed by four cycles feeding N<sub>2</sub>. Ammonia formation was not observed in these first two cycles, while the ammonia formation in the consecutive four cycles was well in line with that observed in Fig. 6(b), when N<sub>2</sub> was fed. This further test thus confirm that ammonia derives from gaseous N<sub>2</sub> rather than N present on the electrocatalyst, at least under the experimental conditions utilized.

Blank tests were also made by feeding N<sub>2</sub>, but without applying the potential, to verify if only a catalytic (rather than electrocatalytic) reaction is present. No ammonia is detected in these experiments. A further blank test was realized by feeding N<sub>2</sub> + H<sub>2</sub>, in order to check again if the applied potential was only necessary to generate H<sub>2</sub> need for the catalytic reaction of N<sub>2</sub> reduction. Also in this case, no ammonia formation was detected. All this series of experiments thus clearly confirm that ammonia formation derives from the electrocatalytic reduction of N<sub>2</sub> and H<sub>2</sub>O, as a further proof from the dependence of the behaviour from the applied potential (Fig. 5).

### 3.6 Nature of the iron species active in the N<sub>2</sub> reduction

In order to understand the nature of the changes during the pre-activation procedure and the possible nature of the iron species active in N<sub>2</sub> direct reduction to ammonia, the Fe<sub>2</sub>O<sub>3</sub>-CNT sample as a function of the activation time was investigated by XPS (X-ray photoelectron spectroscopy). The results are summarized in Fig. 7. No significant differences were observed between the initial electrocatalyst and those after the electrocatalytic tests at -0.5 V, although changes were observed for more negative applied voltages. The XPS spectra in Fig. 7 show in all cases the presence of an O1s signal which may be deconvoluted in four components [44]:

- **O1** (Fe-O-Fe, 530.5±0.1 eV), related to O<sup>2-</sup> in Fe<sub>2</sub>O<sub>3</sub> or FeOOH species;
- **O2** (Fe-O-H, 531.8±0.1 eV), related to FeOOH species;
- **O3** (C-O-C, 532.4±0.1 eV), related to ether functional groups of carbons substrate;
- **O4** (C-O-H, 533.8±0.1 eV), related to OH and COOH functional groups of the carbon substrate.

There is a good fitting of the results which quantification is reported in Table S1 (Supplementary Information). As early commented, the good quality of the fitting tends to exclude the presence of a signal related to oxygen vacancies as reported by Cui et al. [9], i.e. a shoulder at 531.3 eV on the main peak at 530.0 eV related to lattice oxygen in hematite. There is an overlap between the two peaks related to O1 and O2 species, but no indications for a shoulder at 531.3 eV due to lattice oxygen

vacancies is evident. In addition, a peak shift to higher energies of the 711 eV and 724 eV peaks related to Fe  $2p_{3/2}$  and Fe  $2p_{1/2}$  signals, respectively, should be observed upon formation of oxygen vacancies, as shown for example in XPS Fe  $2p$  XPS profile of Fe<sub>2</sub>O<sub>3</sub> before and after sputtering with Ar (Fig. S9(c) in Supplementary Information). The absence of this shift in our case (Fig. S8 - Supplementary Information) excludes that a significant formation of lattice vacancies occurs during the pre-activation process under our experimental conditions. Note also that the Fe  $2p$  XPS spectra of *Fresh Fe<sub>2</sub>O<sub>3</sub>-CNT* and activated samples (Fig. S8 - Supplementary Information) evidence a relative intensification of the satellite Fe  $2p_{3/2}$  and Fe  $2p_{1/2}$  signals (at about 720 and 730 eV, respectively), a slight shift to higher energies of the Fe  $2p_{1/2}$  signal (from about 723.8 to about 724.5) with also a slight narrowing of this peak, all features expected for a change from hematite to maghemite [45] (see Table S2 - Supplementary Information). Thus, XPS data are consistent with the in-situ transformation from hematite to maghemite in Fe<sub>2</sub>O<sub>3</sub>-CNT, rather than with a partial reduction of hematite with the creation of surface oxygen vacancies as indicated for unsupported hematite nanoparticles [9], and to which formation the enhanced activity in N<sub>2</sub> conversion to NH<sub>3</sub> was attributed [9]. The difference in the behaviour is reasonably related to the effect of CNT support and the role of surface CNT defect sites in stabilizing iron-oxide nanoparticles (see Figure S6 in Supplementary Information).

In the data reported in Fig. 7, the total O amount decreases sharply in the *activated 1h* sample with respect to the *fresh Fe<sub>2</sub>O<sub>3</sub>-CNT* sample, while decreases with a lower rate in the following hours of the activation procedure. This is in well agreement with indications discussed before deriving from electron microscopy characterization (Fig. 1). The amount of O3 and O4 species (related to oxygen functional groups on CNT) remains nearly constant with time on stream. The percentage of O2 species (related to FeOOH) in total O1s, increase from 3.8% (*Fresh Fe<sub>2</sub>O<sub>3</sub>-CNT*) to 18% (*Activated 24h*). This suggests an in-situ formation of a ferric oxyhydroxide [FeO(OH), as goethite, i.e.  $\alpha$ -FeO(OH)] species during the electrochemical activation process, although not evidenced by XRD. The data of the deconvolution are reported in Supporting Information (Table S1).

FIGURE 7 HERE

## 4. Discussions

### 4.1 Relationship between XPS O1s signals and rate of ammonia formation

In order to correlate the rate of ammonia formation with the changes of the surface characteristics of the Fe<sub>2</sub>O<sub>3</sub>-CNT electrocatalyst as a function of the activation time, the amount of the different oxygen species was quantified by deconvolution of the XPS O  $1s$  spectra (see Table S1 in Supplementary Information). The results are reported in Figure 8 as a function of the ammonia formation rate of the

iron-based electrocatalysts. The activity of the electrocatalysts towards ammonia synthesis depends linearly on the O1 (Fe-O-Fe) type of oxygen, differently from the other oxygen signals (O2-O4) or the total amount of oxygen. Note that on the bottom of Figure 8 the activation times of the electrocatalysts are indicated, to remark that the rate of ammonia formation passes through a maximum as a function of the activation time, as shown in Fig. 2(b).

#### FIGURE 8 HERE

As commented before, on the contrary, XPS spectra in O 1s and Fe 2p region do not provide evidence of the presence of oxygen vacancies and their relation with the rate of ammonia formation.

The observed linear relationship between the ammonia formation rate and the amount of O1(Fe-O-Fe) species detected by XPS, while not for the other O 1s species, indicates that the species associated to this XPS signal is likely the active one in ammonia synthesis. Although only four points allow to indicate this linear relationship, it must be observed that i) there is a good coefficient of linear correlation, not detected for the other O 1s species, and ii) the linear observation is observed for the same electrocatalyst as a function of the activation time, not for different catalysts, thus limiting the presence of additional possible effects. Based on these considerations, we thus believe that the observed relationship is valid and indicative of a significative correlation between the rate of ammonia formation and the type of iron species present in the electrocatalyst as a function of the time of activation.

#### 4.2 Changes during the activation process and nature of the active iron species

The XPS O1 signal is related to an oxygen atom bridging two iron atoms, as present in Fe<sub>2</sub>O<sub>3</sub> or FeOOH species. Instead no relationship is observed between the rate of ammonia formation and the O2 XPS signal, related to FeO-OH species. The other two oxygen signals (O3, O4) are related to oxygen species present on the functionalized CNT support. The signal at 530 eV (O1) is characteristic of Fe<sub>2</sub>O<sub>3</sub> species [45], but as commented before the change of XPS Fe 2p signal (Fig. S8 - Supplementary part) is indicative of a change from hematite ( $\alpha$ -Fe<sub>2</sub>O<sub>3</sub>) to maghemite ( $\gamma$ -Fe<sub>2</sub>O<sub>3</sub>) species [45], and the XPS O 1s spectrum is also consistent with this interpretation [46]. HRTEM data (Supplementary Information) are also in agreement with the change of the nanostructure from hematite, confirmed by both XRD and TEM data, to magnetite. In the latter case, the iron-oxide species is not detectable, however, by XRD, being nanoparticles too small. Although further results are necessary to confirm this preliminary indication, we feel that XPS and XRTEM data provide a reasonable working hypothesis to explain the significant enhancement of the catalytic behaviour (3–4 times TOF and NH<sub>3</sub> FE) during the first 3 h of electrochemical pre-activation. We could also observe that the results for *activated 3h* sample are among the highest values reported so far for non-

precious metal catalysts that use a continuous-flow polymer-electrolyte-membrane cell and gas-phase operations for the ammonia synthesis hemicell. The electrocatalyst was stable at least 12 h at the working conditions.

These results are significantly different from those observed by Cui et al. [9] using unsupported hematite electrocatalysts, for which a similar in-situ activation effect was observed, but interpreted as due to the formation of oxygen vacancies. Similarly, Jin et al. [8] also proposed that vacancies in 2D layered  $W_2N_3$  nanosheet catalyst are the active sites for NRR, by providing an electron-deficient environment that facilitates nitrogen adsorption and lowers the thermodynamic limiting potential of NRR. In our case, as commented before, XPS data do not indicate the formation of these oxygen vacancies and a possible correlation with the rate of ammonia formation. This is likely due to the effect of CNT. There are clear evidences by HRTEM (Fig. S6 - Supporting Information) that the smaller iron-oxide nanoparticles are strongly interacting with CNT defect sites and that this strong interaction may also changes the shape of the iron-oxide nanoparticles (Fig. S7c - Supporting Information). However, the comparison of the results on the reactivity (Fig. 2b) and distribution of the iron-oxide nanoparticles (Fig. 1) do not indicate a correlation between size of the nanoparticles and behaviour in the direct synthesis of ammonia.

The process occurring during the in-situ electrochemical activation may be thus described as follows. Initially, the electrocatalyst shows a relatively large distribution of mainly hematite ( $\alpha$ - $Fe_2O_3$ ) nanoparticles, with only a small fraction of them small and strongly interacting with CNT defect sites. During the process of in-situ activation, a transformation occurs, with movement of part of the large hematite particles weakly-interacting with CNT to the carbon paper support (removed then during the pre-activation procedure) and the formation also of smaller iron-oxide particles (size  $< 2$  nm) well-interacting with the functionalized sites of o-CNT (oxidized CNT), as shown by TEM. The latter transformation is also associated to the phase transformation from hematite to maghemite. Maghemite has an inverse spinel structure similar to magnetite but has a defective lattice with one ninth of the Fe positions in the lattice being vacant with cell dimension  $a = 8.337\text{\AA}$ . It is likely that these defective lattice sites in maghemite are responsible for the  $N_2$  activation and conversion to ammonia, similar to what proposed by Cui et al. [9] and Jin et al. [8]. It is possible that the interaction of maghemite nanoparticles with CNT defect sites (Fig. S7(c) - Supporting Information) could further enhance the presence of these defective lattice sites on the surface. Therefore, although we observe an apparent different mechanism, the results are in agreement with those of Cui et al. [9] and Jin et al. [8] indicating lattice sites as being responsible for  $N_2$  direct conversion to ammonia.

The removal of nearly half of the initial iron-oxide (during the procedure of activation) does not decrease the activity, but rather improves the formation of ammonia and TOF by at least four times

(Fig. 3) and about three times the FE (Fig. 2b), indicating that the removed species was electroactive, but towards the side reaction of hydrogen formation. However, for times of activation longer than about 3 h, a further evolution of the iron-oxide nanoparticles is observed, with disappearance of the smaller nanoparticles (<2 nm) and formation of nanoparticles with size in the 4–6 nm range (Fig. 1), although still remaining XRD-amorphous. We could suggest the further transformation to magnetite ( $\text{Fe}_3\text{O}_4$ ), although further studies are necessary to characterize better this transformation, which are indeed difficult due to the low amount of iron and the presence of o-CNT. As a further indication, we could indicate that the transformations and spectral features are consistent with indications by Morris et al. [46] regarding the spectral and other physicochemical properties of submicron powders of hematite ( $\alpha\text{-Fe}_2\text{O}_3$ ), maghemite ( $\gamma\text{-Fe}_2\text{O}_3$ ), magnetite ( $\text{Fe}_3\text{O}_4$ ), as well as of goethite ( $\alpha\text{-FeOOH}$ ) and lepidocrocite ( $\gamma\text{-FeOOH}$ ).

As earlier observed by operando XAFS [41] on analogous electrocatalysts, which were used in the electrocatalytic reduction of  $\text{CO}_2$ , an in-situ transformation is observed, driven from the potential applied, of iron-oxide nanoparticles which transform reversibly to an FeOOH (ferrihydrite) species. Operando XAFS [41] also indicates that for more negative applied voltages than -1.5 V, the iron-oxide may reduce to metallic iron, but this transformation enhances the rate of the side reaction of  $\text{H}_2$  formation, with a significant lowering of the selectivity in the reduction of  $\text{CO}_2$ .

Possibly there is a similar process occurring also in this case. The fact that we do not find evidences of the formation of metallic iron in our experimental conditions (Fig. S8 - Supplementary Information) is due to the low applied potential applied, but in agreement, on increasing the negative voltage applied, there is a significant increase in the rate of the side reaction of  $\text{H}_2$  formation (Fig. 5). Thus, it is important to maintain low the overpotential for  $\text{N}_2$  conversion to ammonia.

We earlier suggested [42], by analogy with the reaction mechanism of *Nitrogenase* FeMo-cofactor, that a multi-electron/proton simultaneous transfer to chemisorbed  $\text{N}_2$  to form a  $\text{N}_2\text{H}_2^*$  species, intermediate for  $\text{NH}_3$  formation, is a crucial aspect to avoid the formation of high-energy intermediates and thus maintain low the overpotential in NRR. We also suggested [42] that  $\gamma\text{-FeOOH}$  has a surface configuration resembling the active centers in *Nitrogenase* FeMo-cofactor able to give this multi-electron/proton simultaneous transfer to chemisorbed  $\text{N}_2$ .

Therefore, although this is a preliminary tentative mechanism and further studies are necessary to confirm, this mechanism of surface transformation of iron-oxide species occurring during in-situ activation of  $\text{Fe}_2\text{O}_3\text{-CNT}$  electrocatalysts can well explain the observed relationships between changes of physico-chemical characteristics of the electrocatalyst during in-situ activation and catalytic behaviour in the reduction of  $\text{N}_2$  to ammonia. The in-situ transformation to form maghemite nanoparticles is responsible of the high activity and selectivity in ammonia direct synthesis, possibly

for the reversible in-situ transformation between maghemite and ferrihydrite  $\gamma$ -FeOOH [47]. Maghemite iron-oxide is thus a precursor of the reversible in-situ formation of  $\gamma$ -FeOOH, the active species in  $N_2$  direct electrocatalytic reduction. This is an alternative interpretation with respect to the previous comment on the role of oxygen vacancies in the activation of  $N_2$ . Current data do not allow to discriminate between these two possible reactions mechanisms, also because it is evident that there is a complex dynamic of in-situ transformation of iron-oxide species, which depends on the experimental conditions (applied potential, presence of an electrolyte, specific characteristics of the electrode).

We have also to remark that in addition to formation of the active species, the results presented here further evidence the crucial question of stability of the species generated in-situ. Maghemite nanoparticles, although stabilized at o-CNT defect sites, are not enough thermodynamically stable [48,49] and sinter generating iron-oxide species (such as magnetite -  $Fe_3O_4$ ) for longer times of activation. This transformation reduces the amount of maghemite nanoparticles with a lowering of the activity in ammonia direct synthesis and an enhancement of the side reaction of  $H_2$  formation (lower Faradaic selectivity), although XPS data ( $O_2$  signal) indicates an increase of relative intensity of the oxygen signal related to FeO-OH species. While other species such as  $\alpha/\beta$ -FeOOH (Goethite and Akaganeite, respectively) may form from different iron-oxide species than maghemite ( $\gamma$ - $Fe_2O_3$ ), only the latter generates the  $\gamma$ -FeOOH (Lepidocrocite) active species, or alternatively only the maghemite species contain the defective lattice sites responsible for the  $N_2$  activation and conversion to ammonia.

Although further studies to clarify this working hypothesis are certainly needed, as commented also above, we believe that these results open new perspectives in understanding and optimization of the behaviour of these iron-oxide based electrocatalysts for  $N_2$  direct reduction to ammonia.

## 4. Conclusions

The study of electrochemical pre-activation of  $Fe_2O_3$ -CNT electrocatalysts for ammonia direct synthesis evidence some relevant results. This procedure of pre-activation, leading to an in-situ reconstruction of iron oxide nanoparticles, gives as result a significant increase in the performances, both rate of ammonia formation, TOF and Faradaic selectivity reaching the interesting values of about  $41 \mu g \text{ mg}_{\text{cat}}^{-1} \text{ h}^{-1}$  as rate of ammonia formation and 17% as Faraday efficiency for the electrocatalyst which was activated for 3 h. This corresponds to an increase of nearly twice in the rate of  $NH_3$  formation (about four times on iron oxide weight bases and about five times on current density bases)

and of five time in the Faradaic selectivity. During the activation procedure active sites are created together with a significant elimination of sites responsible for the side reaction of H<sub>2</sub> formation.

The characterization of these electrocatalysts as a function of time of electrochemical activation provides evidences that the electrocatalytic behaviour of Fe<sub>2</sub>O<sub>3</sub>-CNT catalysts in the direct synthesis of ammonia from N<sub>2</sub> is highly depending on the iron-oxide species present on the surface of CNTs during the electrocatalytic reaction, with the tentative indication that maghemite (or its ferrihydrite  $\gamma$ -FeOOH species formed in situ) is the active and selective species for ammonia direct synthesis. More studies are necessary to support further this indication, but it is the first time that evidences about the role of the different iron species in the direct ammonia electrocatalytic synthesis are given, with the suggestion of a peculiar role of the maghemite phase. Two interpretation of this effect are proposed. The first interpretation is that the surface defective lattice sites of maghemite small (< 2 nm) nanoparticles are responsible for the N<sub>2</sub> activation and conversion to ammonia, according to the reaction mechanism proposed by Jin et al. [8] and Cui et al. [9]. These defect lattice sites may be possibly enhanced with respect to unsupported iron-oxide from the strains induced by the strong interaction with CNTs. The second interpretation is that maghemite is generating reversibly during the electrocatalytic reaction the  $\gamma$ -FeOOH (Lepidocrocite) active species, having surface active centres able to promote a simultaneous multi electron/proton transfer according to a reaction mechanism similar to that present in *Nitrogenase* FeMo-cofactor, the only enzyme able to convert N<sub>2</sub> to ammonia.

Present data do not allow to clarify unambiguously the reaction mechanism, but provide working hypotheses on the possible mechanisms and thus the aspect to investigate. We feel that the electrocatalytic mechanism mimicking that present in the *Nitrogenase* enzyme, thus via multi electron/proton simultaneous transfer, is a crucial question to lower the overpotential in NRR and thus minimize the side reaction of H<sub>2</sub> formation. The low observed onset potential in these electrocatalysts (around -0.2–0.3 V, see Fig. S10 - Supplementary Information) is in agreement with this interpretation. However, as indicated, further clarifications are necessary.

The results also remark that stabilization of the in-situ formed species is the necessary step to improve further the properties of these electrocatalysts in the direct synthesis of ammonia from N<sub>2</sub> and H<sub>2</sub>O at room temperature and ambient pressure. These results show how both the activity and selectivity in N<sub>2</sub> direct reduction to ammonia are highly depending on the presence of a specific type of iron-oxide species supported on o-CNT. There is a complex in-situ dynamic of iron-species transformation, and thus the understanding how to stabilize the active species is a clear key to improve the electrocatalysts. We have shown here that stabilization of the iron-oxide active species at defect sites of CNT is an important aspect, but stronger stabilization, by doping the CNT or by using other type of nanocarbon

materials [50] and especially nanocarbons containing hybrid  $sp^2/sp^3$  configurations such as nanodiamonds [51] is a necessary direction to explore.

As final comment we believe that present results also provide indications about the differences between the reaction mechanism in the electrocatalysts for ammonia direct synthesis and in thermal catalytic reaction on fused iron, the commercial ammonia synthesis catalysts. It is evident from the results that an iron-oxide species is active in the electrocatalytic direct reduction of  $N_2$  to ammonia, rather than metallic iron as for thermal catalytic reaction. The consequence is that the reaction mechanism is also different.

In conclusion, the study provides indications on how to improve  $Fe_2O_3$  electrocatalysts for the conversion of  $N_2$  directly to ammonia and also gives preliminary suggestions about the mechanistic aspects of this challenging reaction.

## Acknowledgments

This work was made in the frame of ERC Synergy SCOPE (project 810182) and PRIN 2015 SMARTNESS project nr. 2015K7FZLH projects which are gratefully acknowledged. The work was also co-funded through a SINCHEM Grant. SINCHEM is a Joint Doctorate programme selected under the Erasmus Mundus Action 1 Programme (FPA 2013-0037). The authors thank also Dr. Liyun Zhang and Dr. Yuefeng Liu for the TEM tests.

## Appendix A. Supplementary data

Supplementary data to this article can be found online (file JEC\_Enhanced N2 REVISED SUPPORTING INFO.docx).

## References

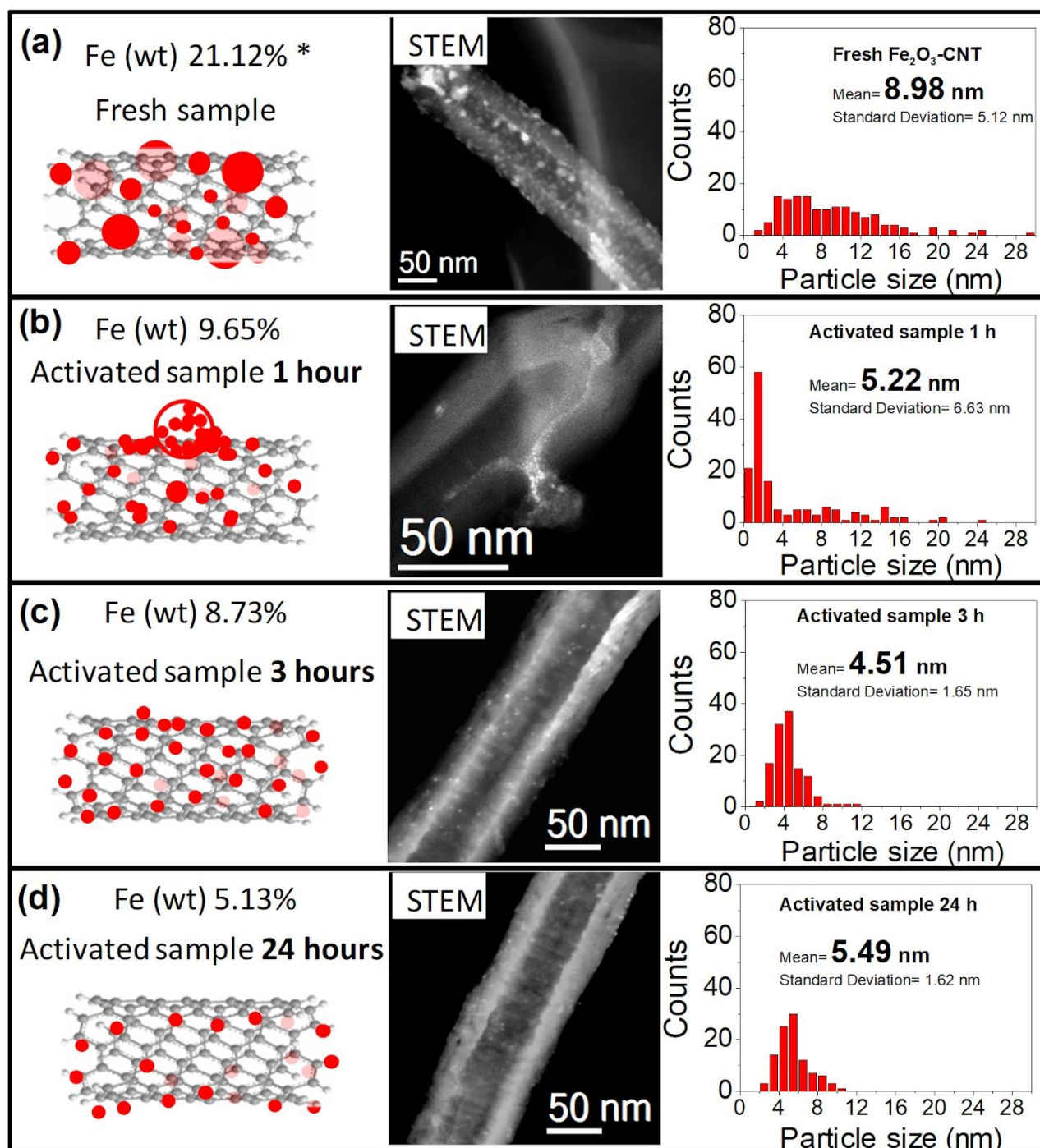
- [1] A. Bazzanella, F. Ausfelder, Low carbon energy and feedstock for the European chemical industry, Dechema Pub.: 60486 Frankfurt am Main, Germany, June 2017.
- [2] J. Ren, A. Yu, P. Peng, M. Lefler, F.-F. Li, S. Licht, *Acc. Chem. Res.*, 52 (2019) 3177-3187.
- [3] S. Giddey, S. P. S. Badwal, C. Munnings, M. Dolan, *ACS Sustainable Chem. Eng.*, 5 (2017) 10231-10239.
- [4] P.H. Pfromm, *J. Renewable and Sustainable Energy*, 9 (2017) 034702.

- [5] (a) P. Lanzafame, S. Abate, C. Ampelli, C. Genovese, R. Passalacqua, G. Centi, S. Perathoner, *ChemSusChem*, 10 (2017) 4409-4419. (b) G. Centi, G. Iaquaniello, S. Perathoner, *BMC Chem. Eng.*, 1 (2019) 5/1-16.
- [6] A. P. O'Mullane, M. Escudero-Escribano, I. E. L. Stephens, K. Krischer, *ChemPhysChem*, 20 (2019) 2900 – 2903.
- [7] C. Tang, S.-Z. Qiao, *Chem. Soc. Rev.*, 48 (2019) 3166-3180.
- [8] H. Jin, L. Li, X. Liu, C. Tang, W. Xu, S. Chen, L. Song, Y. Zheng. S.-Z. Qiao, *Advan. Mater.*, 31 (2019) 1902709.
- [9] X. Cui C. Tang, X. - M. Liu, C. Wang, W. Ma, Q. Zhang, *Chem. A Eur. J.*, 24 (2018) 18494-18501.
- [10] Q. Wang, J. Guo, P. Chen, *J. Energy Chem.*, 36 (2019) 25-36.
- [11] X. Guo, Y. Zhu, T. Ma, *J. Energy Chem.*, 26 (2017) 1107-1116.
- [12] J. Yang, W. Weng, X. Wei, *J Energy Chem.*, 43 (2020) 195-207.
- [13] B. H. R. Suryanto, H.-L. Du, D. Wang, J. Chen, A. N. Simonov, D. R. MacFarlane, *Nature Catal.*, 2 (2019) 290–296.
- [14] J. Deng, J. A. Iniguez, C. Liu, *Joule* 2 (2018) 846–856.
- [15] L. Wang, M. Xia, H. Wang, K. Huang, C. Qian, C. T. Maravelias, G. A. Ozin, *Joule*, 2 (2018) 1055–1074.
- [16] V. Kyriakou, I. Garagounis, E. Vasileiou, A. Vourros, M. Stoukides, *Catal. Today*, 286 (2017) 2-13
- [17] M. Jewess, R. H. Crabtree, *ACS Sustainable Chem. & Eng.*, 4 (2016) 5855 -5858.
- [18] M. A. Shipman, M. D. Symes, *Catal. Today*, 286 (2017) 57-68.
- [19] D. Bao, Q. Zhang, F. L. Meng, H. X. Zhong, M. M. Shi, Y. Zhang, J. M. Yan, Q. Jiang, X. B. Zhang, *Adv. Mater.*, 29 (2017) 1604799.
- [20] J. H. Montoya, C. Tsai, A. Vojvodic, J. K. Norskov, *ChemSusChem*, 8 (2015) 2180-2186.
- [21] Y. Tanabe, Y. Nishibayashi, *Coord. Chem. Rev.*, 257 (2013) 2551-2564.
- [22] C. Lv, Y. Qian, C. Yan, Y. Ding, Y. Liu, G. Chen, G. Yu, *Angew. Chem. Int. Ed.*, 57 (2018) 10246-10250.
- [23] L. Zhang, L. X. Ding, G. F. Chen, X. Yang, H. Wang, *Angew. Chem. Int. Ed.*, 58 (2019) 2612-2616.
- [24] H. Wang, L. Wang, Q. Wang, S. Ye, W. Sun, Y. Shao, Z. Jiang, Q. Qiao, Y. Zhu, P. Song, D. Li, L. He, X. Zhang, J. Yuan, T. Wu, G. A. Ozin, *Angew. Chem. Int. Ed.*, 57 (2018) 12360-12364.

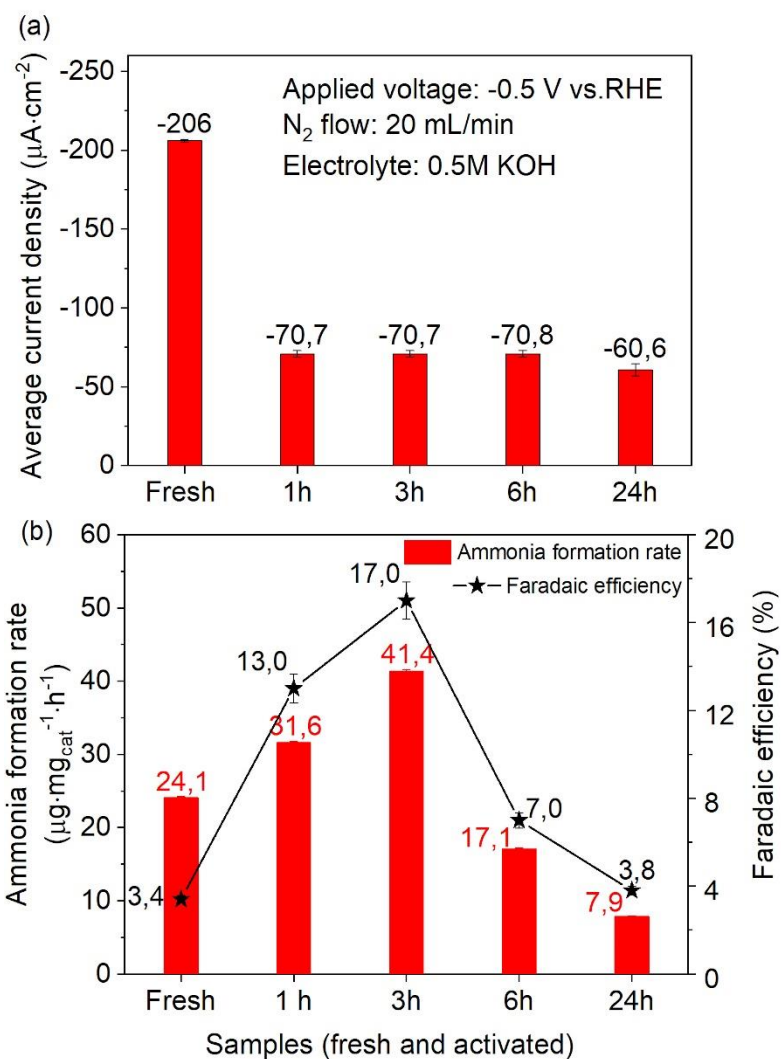
- [25] L. Han, X. Liu, J. Chen, R. Lin, H. Liu, F. Lu, S. Bak, Z. Liang, S. Zhao, E. Stavitski, J. Luo, R. R. Adzic, H. L. Xin, *Angew. Chem. Int. Ed.*, 58 (2019) 2321-2325.
- [26] R. Zhao, H. Xie, L. Chang, X. Zhang, X. Zhu, X. Tong, T. Wang, Y. Luo, P. Wei, Z. Wang, X. Sun, *EnergyChem*, 1 (2019), 100011.
- [27] A. J. Martín, T. Shinagawa, J. Pérez-Ramírez, *Chem*, 5 (2019) 263-283.
- [28] B. Xua, Z. Liu, W. Qiu, Q. Liu, X. Sun, G. Cui, Y. Wu, X. Xiong, *Electrochimica Acta*, 298 (2019) 106-111.
- [29] Y.-J. Shih, Y.-H. Huang, C.P Huang, *Electrochimica Acta*, 263 (2018) 261-271.
- [30] A.Chen, B. Yu Xia, *J. Mater. Chem. A*, 7 (2019) 23416-23431.
- [31] S. Giddey, S. P. S. Badwal, A. Kulkarni, *Int. J. Hydrogen Energy*, 38 (2013) 14576-14594.
- [32] G. Hochman, A. S. Goldman, F. A. Felder, J. M. Mayer, A. J. M. Miller, P. L. Holland, L. A. Goldman, P. Manocha, Z. Song, S. Aleti, *ChemRxiv* (2019), 1-26.
- [33] I. J. McPherson, T. Sudmeier, J. Fellowes, S.C.E. Tsang, *Dalton Trans.*, 48 (2019) 1562-1568.
- [34] a) S. Chen, S. Perathoner, C. Ampelli, C. Mebrahtu, D. Su, G. Centi, *Angew. Chemie Int. Ed.*, 56 (2017) 2699-2703; b) S. Chen, S. Perathoner, C. Ampelli, C. Mebrahtu, D. Su, G. Centi, *ACS Sustainable Chem. & Eng.*, 5 (2017) 7393-7400; c) S. Chen, S. Perathoner, C. Ampelli, G. Centi, *Studies in Surface Science and Catal.*, 178 (2019) 31-46.
- [35] T. Kandemir, M. E. Schuster, A. Senyshyn, M. Behrens, R. Schlögl, *Angew. Chem.-Int. Edit.*, 52 (2013) 12723-12726.
- [36] T. Kandemir, M. E. Schuster, A. Senyshyn, M. Behrens, R. Schlögl, *Angew. Chemie Int. Ed.*, 52 (2013) 12723-12726
- [37] A. L. Garden, E. Skúlason, *J. Phys.Chem. C*, 119 (2015) 26554-26559.
- [38] M. Ouzounidou, A. Skodra, C. Kokkofitis, M. Stoukides, *Solid State Ionics*, 178 (2007) 153-159.
- [39] A. R. Singh, B. A. Rohr, J. A. Schwalbe, M. Cargnello, K. Chan, T. F. Jaramillo, I. Chorkendorff, J. K. Nørskov, *ACS Catal.*, 7 (2017) 706-709.
- [40] a) B. M. Hoffman, D. Lukoyanov, Z. Y. Yang, D. R. Dean, L. C. Seefeldt, *Chem. Rev.*, 114 (2014) 4041-4062; b) B. M. Hoffman, D. Lukoyanov, D. R. Dean, L. C. Seefeldt, *Acc. Chem. Re.s*, 46 (2013) 587-595.
- [41] C. Genovese, M. E. Schuster, E. K. Gibson, D. Gianolio, V. Posligua, R. Grau-Crespo, G.Cibin, P. P. Wells, D. Garai, V. Solokha, S. K. Calderon, J. J. Velasco-Velez, C. Ampelli, S. Perathoner, G. Held, G. Centi and R. Arrigo, *Nature Comm.*, 9 (2018) 935.
- [42] S. Perathoner, G. Centi, *Catal.Today*, 330 (2019) 157-170.

- [43] a) B. Zhang, W. Zhang, D. S. Su, *ChemCatChem* 2011, 3, 965-968. b) B. Zhang, W. Zhang, D. S. Su, *Microscopy and Analysis* 2012, 26, 15-20.
- [44] a) R. Arrigo, M. Hävecker, S. Wrabetz, R. Blume, M. Lerch, J. McGregor, E. P. Parrott, J. A. Zeitler, L. F. Gladden, A. Knop-Gericke, *J. Amer. Chem. Soc.* 2010, 132, 9616-9630; b) D. S. Su, S. Perathoner, G. Centi, *Chem. Rev.* 2013, 113, 5782-5816; c) D. S. Su, J. Zhang, B. Frank, A. Thomas, X. Wang, J. Paraknowitsch, R. Schlögl, *ChemSusChem* 2010, 3, 169-180.
- [45] T. Radu, C. Iacovita, D. Benea, R. Turcu, *Applied Surface Science* 405 (2017) 337-343.
- [46] N. S. McIntyre, D. G. Zetaruk, *Anal. Chem.* 1977, 49, 1521-1529.
- [46] R. V. Morris, H. V. Lauer Jr., C. A. Lawson, E. K. Gibson Jr., G. A. Nace, C. Stewart, *J. Geophys. Res.: Solid Earth* 1985, 90, 3126-3144.
- [47] V. Barron, J. Torrent, *Geochimica et Cosmochimica Acta* 2002, 66, 2801–2806.
- [48] T. W. Swaddle, P. Oltmann, *Can. J. Chem.* 1980, 58, 1763-1772.
- [49] U. Schwertmann, J. Friedl, H. Stanjek, *J. Colloid and Interface Science* 1999, 209, 215-223.
- [50] D. S. Su, S. Perathoner, G. Centi, *Chem. Rev.*, 113 (2013) 5782–5816.
- [51] Y. Lin, X. Sun, D. S. Su, G. Centi, S. Perathoner, *Chem. Soc. Rev.*, 47 (2018) 8438--8473.

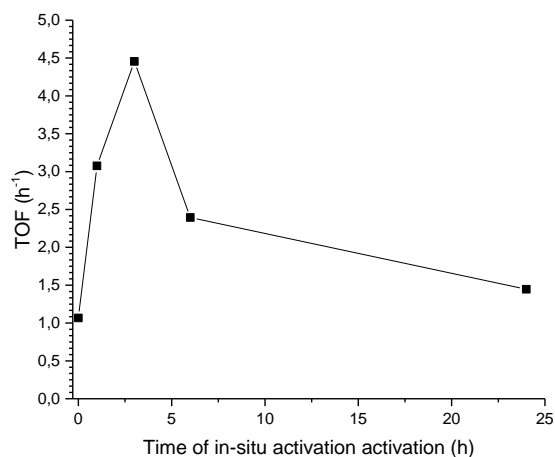
## FIGURES



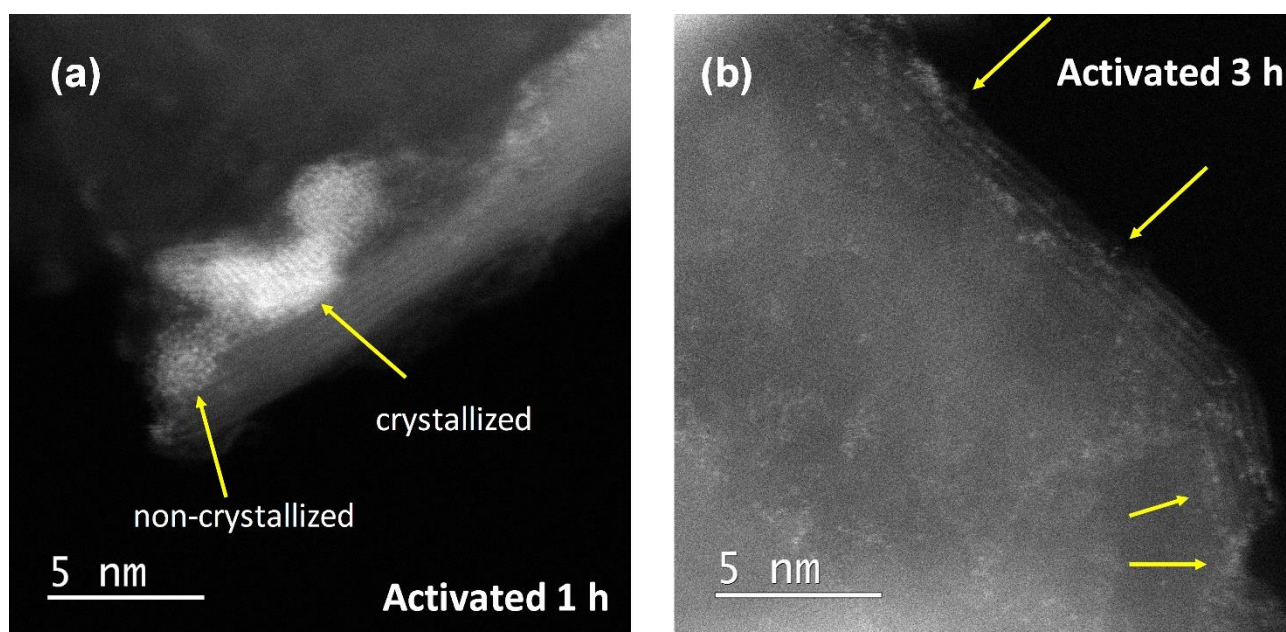
**Fig. 1.** Scanning transmission electron microscopy (STEM) and particle size distribution (PSD) of electrocatalysts: (a) Fresh Fe<sub>2</sub>O<sub>3</sub>-CNT, (b) activated 1 h, (c) activated 3 h, and (d) activated 24 h. The weight amount of iron-oxide is determined by EDX. \* Quantified by XPS and confirmed by AAS.



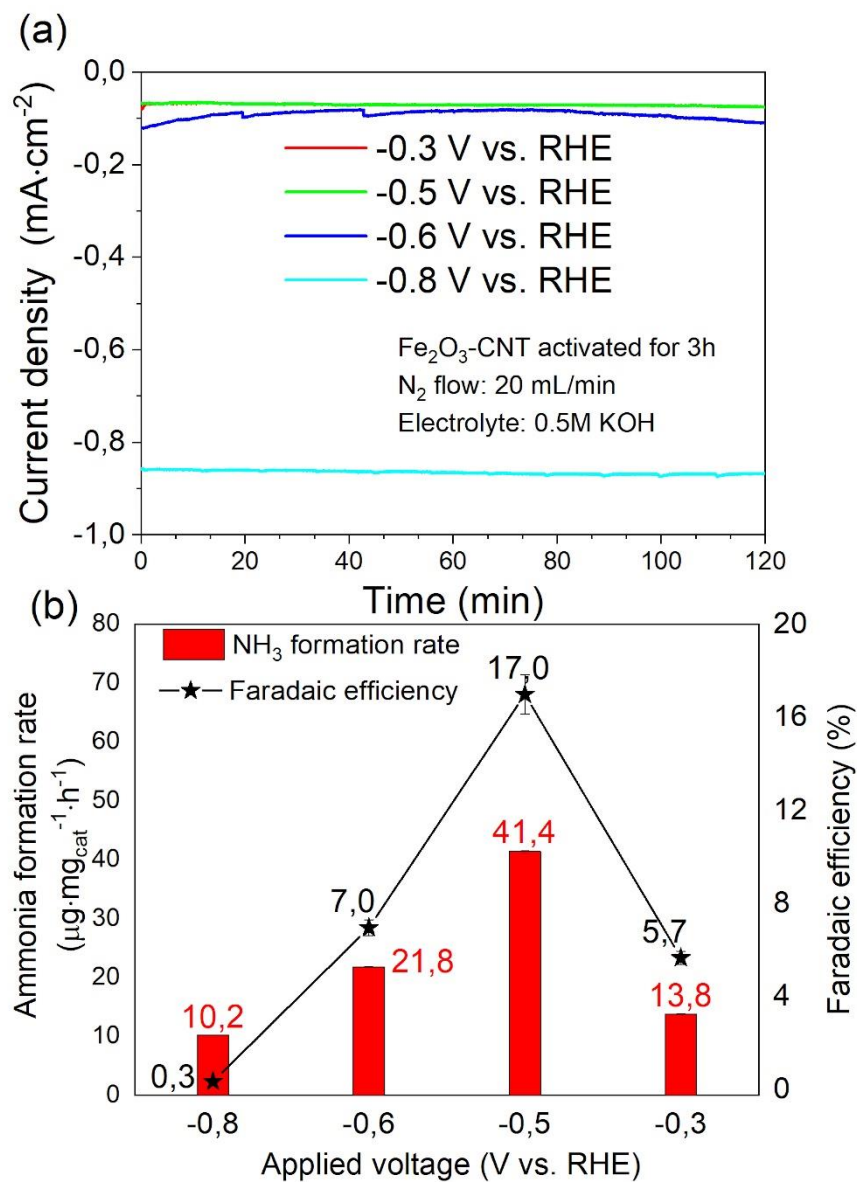
**Fig. 2.** Electrocatalytic performances of Fresh  $\text{Fe}_2\text{O}_3$ -CNT samples and activated 1 h, 3 h, 6 h and 24 h at applied voltage of -0.5 V vs. RHE: (a) current density; (b) ammonia formation rate and Faradaic efficiency.



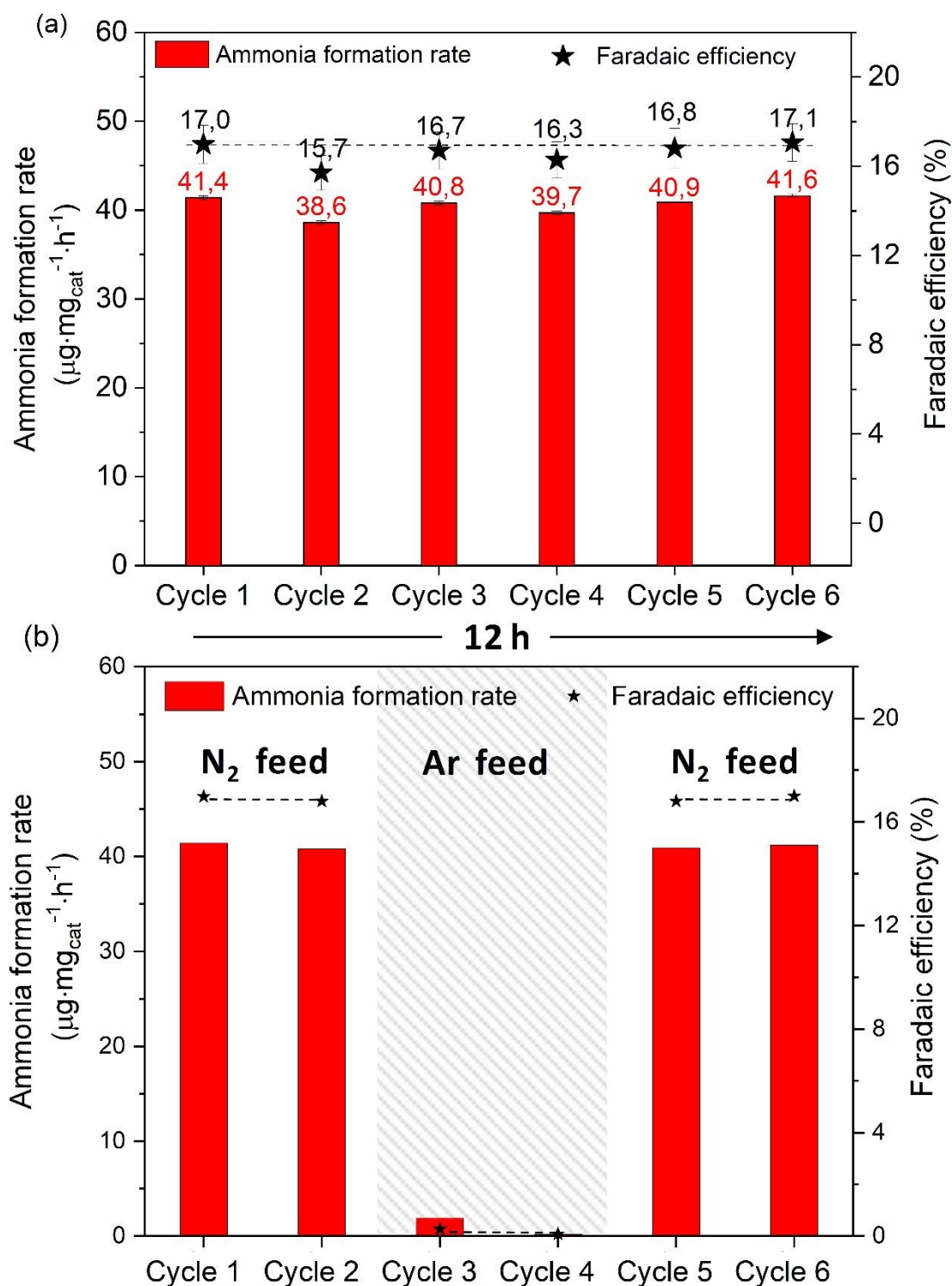
**Fig. 3.** Apparent Turnover Frequency (TOF), estimated by assuming that all iron atoms are active in the N<sub>2</sub> reduction, as a function of the time of in-situ activation of the electrocatalysts.



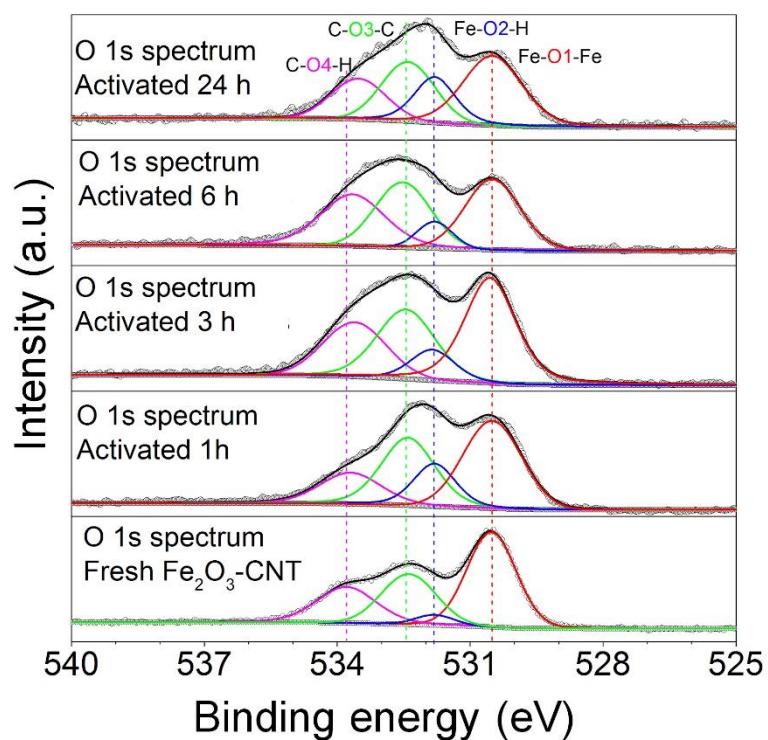
**Fig. 4.** (a) HRTEM of activated 1 h sample showing the reconstruction process of the crystallized iron oxide; (b) HRTEM of activated 3 h sample showing that the non-crystallized iron oxide is located at the edge or defect of CNT.



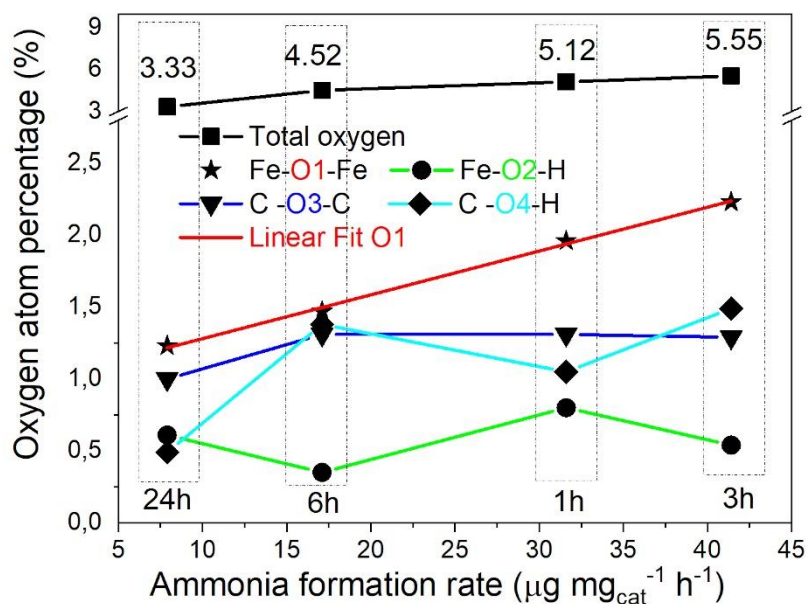
**Fig. 5.** Electrocatalytic performances of activated 3h sample at different applied voltages. (a) Current density; (b) ammonia formation rate and Faradaic efficiency.



**Fig. 6.** (a) Stability tests: ammonia formation rate and Faradaic selectivity during a series of consecutive cycles (each of 120 min), test conditions as in Fig. 5 (-0,5 V applied voltage vs. RHE). (b) Switch tests between  $\text{N}_2$  and argon in a new series of test cycles, other conditions as in Fig. 6(a). Electrocatalyst activated 3 h.

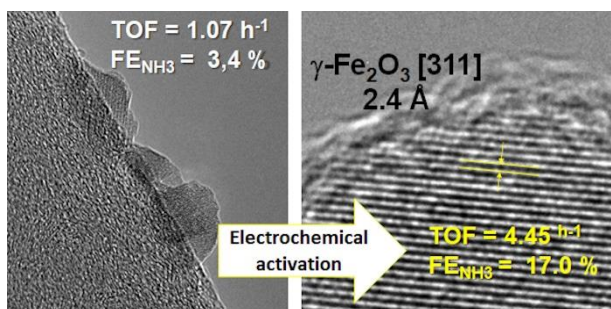


**Fig. 7.** O 1s XPS spectra of Fresh Fe<sub>2</sub>O<sub>3</sub>-CNT samples and activated 1 h, 3 h, 6 h and 24 h.



**Fig. 8.** The relationship observed between the different O 1s species and total oxygen amount detected by XPS and the ammonia formation rates for different activated time samples at an applied voltage of -0.5 V vs. RHE.

### Graphical Abstract:



Electrochemical method to prepare high performance catalysts for direct synthesis of ammonia from N<sub>2</sub> and H<sub>2</sub>O at ambient temperature/pressure.